Amide Exchange Shows Calcium-Induced Conformational Changes Are Transmitted to the Dimer Interface of S100B†

Nicole M. Marlatt and Gary S. Shaw*

Department of Biochemistry, The University of Western Ontario, London, Ontario, Canada N6A 5C1

Received December 21, 2006; Revised Manuscript Received April 17, 2007

ABSTRACT: S100B is a 21 kDa member of the S100 calcium-binding protein family. This protein comprises a symmetric homodimer with each subunit having two EF-hands arranged from four α-helices (I−IV). S100B binds calcium and undergoes a conformation change leading to the exposure of hydrophobic surface residues that enable the protein to interact with biological target molecules. The most significant structural change that occurs during calcium binding results in a change in the orientation of helix III with respect to helices II and IV. In this work, the calcium-sensitive conformational change has been studied by utilizing fast $^{1}H-^{15}N$ HSQC experiments and water-transfer methods to follow the amide exchange in apo-S100B and Ca-S100B at 35 °C. In apo-S100B, the protection factors are 2−3 orders of magnitude lower for helix III than for helix I, II, or IV. In addition, the exchange stability measured here for the dimer interface helices (I, I′, IV, and IV′), in the absence of calcium, is similar to the stability obtained from chemical denaturation experiments. When calcium binds, significant decreases in the protection factors for helices I and IV indicate a modification in the stability of the dimer interface has occurred. In contrast, helix II protection factors increase slightly, which is consistent with a decreased level of surface exposure of this helix. These data have been compared with those of the monomeric S100 protein, calbindin D_{9k}, to illustrate that upon calcium binding there is a balance maintained between the amide exchange rates in helices II and III, although largely the rates are dissimilar for each of these proteins. This distinguishing feature may be important for the calcium-induced conformational change in S100B, where calcium binding is transmitted to the dimer-forming helices.

The S100 proteins are members of the EF-hand calcium-binding protein family. These dimeric proteins possess two helix−loop−helix calcium-binding sites within each monomer comprised of helices I and II in site I and helices III and IV in site II, which are separated by an extended linker region. In general, the S100 proteins are cell specific and have important roles in calcium signaling (*1*, *2*). For example, S100B[1] controls the assembly of the cytoskeletal proteins tubulin (*3*−*5*), glial fibrillary acidic protein (*6*, *7*), and vimentin (*4*) in a calcium-sensitive manner. In addition, S100 proteins have been implicated in disease processes such as Alzheimer's (*8*, *9*) and rheumatoid arthritis (*10*). In all cases, the calcium-induced conformational changes and the mechanism of action of the S100 proteins appear to be different from those of other EF-hand signaling members such as the muscle protein troponin C (*11*) and the multifunctional protein calmodulin (*12*). Three-dimensional structures of S100B (*13*−*17*), S100A6 (*18*−*22*), and S100A11 (*23*) indicate that these proteins undergo a significant conformational change in site II upon calcium binding, exposing several hydrophobic residues that are required for interaction with biological targets (Figure 1). Studies of S100B indicate that helices III and IV and the linker region between helices II and III are important for protein−protein interactions (*24*−*26*), whereas in S100A10 and S100A11, helix I, helix IV, and the linker region have been shown to interact with annexin I and II, respectively (*23*, *27*).

A unique feature of the S100 proteins that distinguishes them from traditional EF-hand calcium-binding proteins such as calmodulin and troponin C is their ability to form both homodimers and heterodimers in vivo. Three-dimensional structures of several homodimeric S100 proteins (*13*−*22*, *28*) have provided important details about the dimer interface of these proteins, the most structurally conserved region in the S100 proteins. Specifically, the interface is composed of helices I and IV from one monomer and helices I′ and IV′ from the second monomer (Figure 1). The conserved nature of many of the residues in helices I and IV indicates that specific residues in these helices play an important structural role in the maintenance of the dimeric structure and a lesser role in the calcium-induced conformational change or calcium-sensitive protein interactions (*21*, *29*). Less well understood is a rationale for the 1000-fold difference in the dimerization of S100B (K_d < 1 nM) compared to that of either S100P ($K_d \sim 2$ μM) or S100A4 ($K_d \sim 4$ μM). The most divergent member of the S100 family is calbindin D_{9k}.

† This research was supported by research and maintenance grants from the Canadian Institutes of Health Research (G.S.S.), an award from the Canada Research Chairs Program (G.S.S.), and an Ontario Graduate Scholarship in Science and Technology (N.M.M.).

* To whom correspondence should be addressed: Department of Biochemistry, University of Western Ontario, London, Ontario N6A 5C1, Canada. Phone: (519) 661-4021. Fax: (519) 661-3175. E-mail: gshaw1@uwo.ca.

[1] Abbreviations: NMR, nuclear magnetic resonance; HSQC, heteronuclear single-quantum correlation; apo-S100B, calcium-free S100B protein; Ca-S100B, calcium-bound S100B; Ca-calbindin D_{9k}, calcium-bound calbindin D_{9k}; CLEANEX-PM, phase-modulated clean chemical exchange; ΔPF, difference in log protection factor between calcium-bound and calcium-free (apo) proteins.

10.1021/bi6026242 CCC: $37.00
Published on Web 05/31/2007

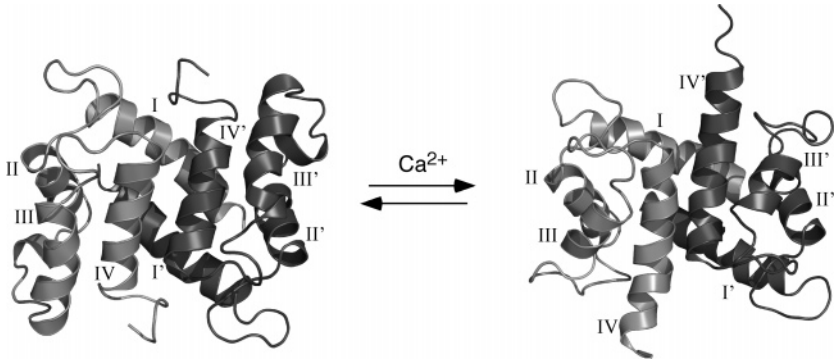

FIGURE 1: Representative structures of an apo and calcium-bound S100 protein. The ribbon diagrams shown are bovine apo-S100B (left) (*17*) and human Ca-S100B (right) (*13*). For each structure, the two monomers are shaded differently and symmetrical helices in the dimers are labeled accordingly (i.e., I, I′). Comparison between apo-S100B (left) and Ca-S100B (right) reveals that calcium binding leads to a reorientation of helix III.

This protein is shorter (75 residues), exists as a monomer, and has an ~1000-fold higher affinity for calcium than other S100 members (*30*). The higher calcium affinity of calbindin D_{9k} is required for the tight regulation of calcium concentrations in the cell. As a result, calbindin D_{9k} undergoes only minimal structural changes upon binding calcium, leading to a repacking of helices III and IV rather than the large conformational changes exhibited by proteins such as S100B and S100A11.

Detailed three-dimensional structures of calcium-binding proteins have provided insight into the way that calcium-binding proteins respond to calcium. In addition, dynamics studies can provide detailed information about the instability and flexibility of a protein that may be important for their biological function. Several studies have examined the fast internal dynamics (picosecond to nanosecond) of EF-hand calcium-binding proteins using ^{15}N and ^{13}C relaxation measurements (*31*−*37*). These experiments have shown that fast internal motions, especially in the calcium-binding sites, exist more in the calcium-free state than in the calcium-bound state and may be a necessary property for the promotion of calcium binding. However, very little information about slower time scale motions (microseconds and slower) in calcium-binding proteins provided by amide exchange experiments is available (*38*, *39*). These investigations may be particularly important for the S100 proteins to establish the mechanisms of calcium binding, the stability of the dimeric structure, and the flexibility of the helices.

The work presented here uses amide exchange experiments measured by NMR spectroscopy to probe the residue accessibility and stability of human S100B in both the calcium-free (apo) and calcium-bound states. These are the first such experiments carried out on a dimeric S100 calcium-signaling protein. Further, we have evaluated correlations found between our data and amide exchange rates measured for the monomeric S100 protein, calbindin D_{9k} (*39*). Our results show that the effects of calcium binding on S100B are transmitted to helices I and IV at the dimer interface of the protein, indicative of a direct link between dimerization and calcium binding in the S100 proteins.

EXPERIMENTAL PROCEDURES

Protein Labeling and Purification. Expression and purification of human S100B were conducted as previously described (*40*). In short, uniformly ^{15}N-labeled human S100B was synthesized by expression in *Escherichia coli* strain N99 using M9 minimal medium. The expression procedure for S100B results in a population of the N-terminal methionine-containing protein that remains uncleaved. Purification of ^{15}N-labeled S100B yielded a single band by gel electrophoresis comprising three chemically different forms of S100B. These have been identified and characterized as formyl-methionine S100B, desformyl S100B, and desmethionine S100B using both electrospray mass spectrometry and NMR spectroscopy (*41*).

NMR Spectroscopy. All NMR experiments were conducted at 35 °C on a Varian Unity 500 MHz spectrometer or an Inova 600 MHz spectrometer, each equipped with a triple-resonance probe and z-field gradients. Sequential assignments of apo-S100B and Ca-S100B were completed using standard HNCA (*42*), HNCO (*43*), HNCACB (*44*), and ^{15}N TOCSY-HSQC (*45*) experiments. Sensitivity-enhanced $^{1}H-^{15}N$ HSQC spectra (*46*) for apo-S100B were acquired using carrier frequencies of 4.73 (^{1}H) and 120 ppm (^{15}N) and spectral widths of 7000.4 and 1500.0 Hz, respectively. Similar spectra were generated for Ca-S100B by using carrier frequencies of 4.68 (^{1}H) and 117.9 ppm (^{15}N) and spectral widths of 6999.7 and 1230 Hz, respectively. All spectra were processed with NMRPipe (*47*) using a cosine-squared function in ^{1}H and ^{15}N to minimize artifacts in the spectra. Apo-S100B data were forward predicted in F_1 to double the number of data points, zero-filled to 4096 points in F_2 and 512 points in F_1, and baseline corrected. Ca-S100B $^{1}H-^{15}N$ HSQC spectra were processed in the same way, except that in F_1 zero filling to 1024 points was used.

Sample Preparation for Amide Exchange Experiments. A 1 mM solution of ^{15}N-labeled apo-S100B in 50 mM KCl and a 90% H_2O/10% D_2O mixture was prepared at pH 6.96. Two-dimensional $^{1}H-^{15}N$ HSQC (*46*) NMR spectra were recorded using 16 steady-state transients, one transient per increment, a recycle delay of 0.9 s, and 64 complex points in t_1 for a total acquisition time of 156 s per spectrum. For Ca-S100B, a 1 mM ^{15}N-labeled S100B solution in 50 mM KCl, a 90% H_2O/10% D_2O mixture, and excess $CaCl_2$ was prepared at pH 7.20. NMR spectra were recorded using 16 steady-state transients, four transients per increment, a recycle delay of 1.0 s, and 32 complex points in t_1 for an acquisition time of 304 s per spectrum. Initial reference spectra of both samples were collected in a 90% H_2O/10% D_2O mixture. The samples were lyophilized and rapidly redissolved in D_2O

at 35 °C. The time required for mixing and placement of the sample into the NMR spectrometer, prior to acquisition for apo-S100B, was 110 s for the pH 6.96 sample. A total of 42 spectra were then collected on this sample at 35 °C. For Ca-S100B, preparation of the sample and placement within the NMR spectrometer took 520 s, at which time the first of 23 spectra was recorded.

Data Analysis for Amide Exchange Experiments. Data were analyzed using PIPP/STAPP (*48*) or NMRView (*49*). The first spectrum of each amide exchange series was picked and identified. Subsequent spectra were automatically peak-picked in combination with complete chemical shift assignments for human apo-S100B (S. Malik and G. S. Shaw, unpublished experiments) or Ca-S100B (*50*). Each spectrum was visually checked for correctness during the peak-picking process. The peak intensities, measured during peak-picking, were tabulated and fit for a single-exponential decay of the form

$$I_t = I_o e^{-kt} \quad (1)$$

where I_o is the original peak intensity, I_t is the intensity at time t, and k is the amide exchange rate constant. In cases where severe overlap of two resonances was noted from the reference $^1H-^{15}N$ HSQC spectra, and where it became clear that "fast" and "slow" rate constants were giving rise to the decay, a sum of exponential curves was used to fit the data. NMR data processing was performed using Xcrvfit (www.bionmr.ualberta.ca/bds/software/xcrvfit) on a Sun Ultra10 computer.

CLEANEX-PM Experiments. Water−amide proton exchange rates for both apo-S100B and Ca-S100B were determined by the CLEANEX-PM method (*51*) at 600 MHz using a 5.88 kHz ^1H spin lock. Samples were made with 2 mM uniformly ^{15}N-labeled S100B in 50 mM KCl and a 90% H_2O/10% D_2O mixture prepared at pH 7.20. For Ca-S100B, an excess of $CaCl_2$ was added to the sample to ensure all calcium-binding sites were occupied with this ion. Duplicate data sets were acquired for apo-S100B using 64 steady-state transients, 64 transients per increment, a recycle delay of 2.0 s, and 64 complex points in t_1. Reference spectra for each sample were collected using the (CLEANEX-PM)-FHSQC pulse sequence (*51*). A series of six spectra were recorded for apo-S100B at mixing times (τ_m) of 5, 10, 20, 30, 40, and 60 ms. An analogous series was collected for the Ca-S100B sample with the addition of three longer mixing times of 80, 100, and 120 ms.

Data Analysis for CLEANEX-PM Experiments. Peak assignments and peak intensities were determined by the same method previously described for the amide exchange data. Rate constants for exchange (k_{ex}) were obtained by using the following equation (*51*):

$$I/I_{ref} = k_{ex}/(R_{1a} + k_{ex} - R_{1B}) \times \{\exp(-R_{1B}\tau_m) - \exp[-(R_{1a} + k_{ex})\tau_m]\} \quad (2)$$

where I_{ref} is the peak intensity from the reference spectra, I is the peak intensity at mixing time τ_m, k_{ex} is the exchange rate constant, and R_{1a} is a combination of longitudinal and transverse relaxation rates. The dependence of the water signal (R_{1B}) on mixing time was measured using a one-dimensional CLEANEX-PM experiment as described previously (*52*) and found to be 2.0 s^{-1}. Equation 2 was fit for the normalized rate constants, k_{ex}, using GraphPad (San Diego, CA) Prism (Macintosh version 4.0a) and corrected for water saturation effects (*51*).

Exchange rates for amides that were below the detection limit of the CLEANEX-PM experiments or disappeared prior to the first amide exchange spectrum were approximated using the method of Skelton and co-workers (*39*). This was only the case for select residues in Ca-S100B as all residues for apo-S100B could be measured by either slow amide exchange or the CLEANEX-PM method. Minimum observable cross-peak intensities in the first $^1H-^{15}N$ HSQC spectrum collected after D_2O addition were conservatively estimated to have decreased >26-fold in the pre-acquisition period, providing a lower limit for amide exchange (k_{ex}) of 4.0×10^{-3} s^{-1} at pH 7.20.

Protection Factor Calculations. The protection factors for each amide were calculated from the k_{rc}/k_{ex} ratio for the measured exchange (k_{ex}) and the calculated intrinsic rate constant (k_{rc}) (*53*). The intrinsic rates for S100B were calculated using the equation

$$k_{rc} = k_{A,ref}(A_L A_R)[D^+] + k_{B,ref}(B_L B_R)[OD^-] + k_{W,ref}(B_L B_R) \quad (3)$$

where $k_{A,ref}$, $k_{B,ref}$, and $k_{W,ref}$ are the reference rates for acid, base, and water catalysis, respectively, of a poly-D,L-alanine peptide under low-salt conditions and A_L, A_R, B_L, and B_R are acid or base side chain specific correction factors. All reference rates were adjusted to 35 °C, the temperature used for backbone amide exchange experiments for both apo-S100B and Ca-S100B. Differences in protection factors (ΔPF) between calcium-free and calcium-bound S100B and calbindin D_{9k} proteins were calculated according to the equation ΔPF = [log protection factor(Ca protein) − log protection factor(apoprotein)].

RESULTS AND DISCUSSION

The three-dimensional structures of human apo-S100B (S. Malik and G. S. Shaw, unpublished), rat apo-S100B (*16*), bovine apo-S100B (*17*), rabbit apo-S100A6 (*19*, *22*), human apo-S100A3 (*28*), rat S100A1 (*54*), rabbit apo-S100A11 (*55*), human apo-S100A4 (*56*), and human S100P (*57*) have been determined using either NMR spectroscopy or X-ray crystallography. The structure of bovine apo-S100B in Figure 1 is representative of these apo-S100 proteins comprising four α-helices (I−IV), two calcium-binding loops, and a linker region (between helices II and III) within each monomer. The dimer interface in the S100 proteins is formed via an X-type bundle arrangement of helices I and IV from one monomer with helices I′ and IV′ of its partner. When calcium binds, a conformational change in helix III in site II (Figure 1) occurs to facilitate binding of a variety of biological targets (*58*).

Identification of Exchanging Backbone Amides. Complete ^{15}N and H^N assignments for human apo-S100B (S. Malik and G. S. Shaw, unpublished experiments) and Ca-S100B (*50*) were obtained using standard triple-resonance experimental approaches. The $^1H-^{15}N$ HSQC spectrum of human apo-S100B (Figure 2A) shows that 82 of 91 $^1H-^{15}N$ correlations are resolved. Multiple resonances for residues

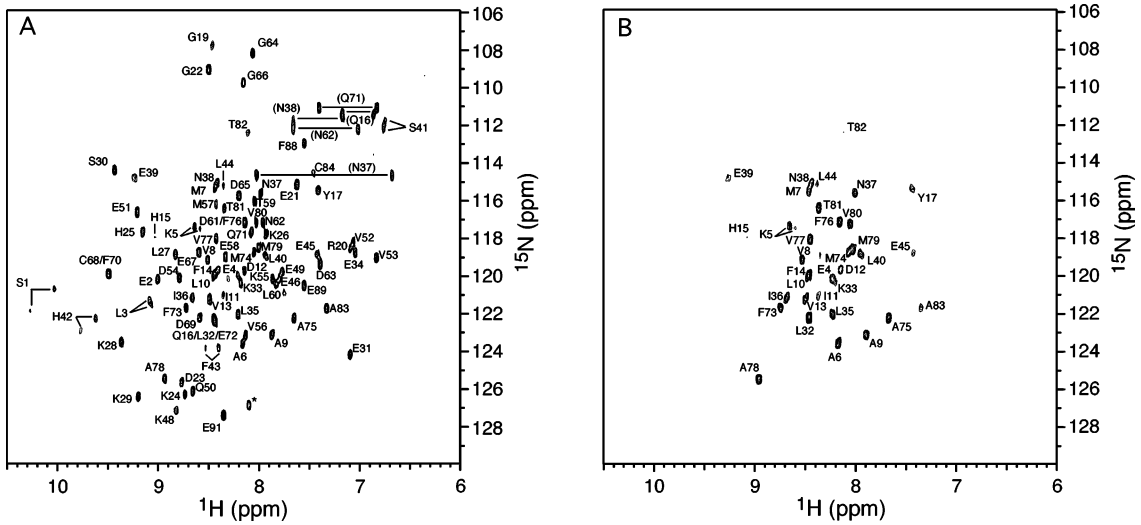

FIGURE 2: $^{1}H-^{15}N$ HSQC spectra of 1 mM ^{15}N-labeled recombinant human apo-S100B at pH 6.96 and 35 °C. Each spectrum is labeled with the amino acid number and letter code. Multiple forms (formyl-methionine and desformyl-methionine, described in the text) are indicated with connecting lines for S1, L3, K5, S41, H42, and F43, and the asterisk represents Met0. Spectrum A was acquired in a 90% H_2O/10% D_2O mixture immediately prior to deuterium exchange. Spectrum B was acquired after lyophilization of the sample used for panel A, the sample being redissolved in D_2O, and exchanged for 10 h at a constant temperature of 35 °C. Each spectrum was acquired using a single transient for 64 complex t_1 points yielding an acquisition time of 156 s.

S1, L3, K5, and A6 in helix I and S41, H42, and F43 in the linker region are noted in the spectrum. This multiplicity results from differential N-terminal modification of S100B so that both formyl-methionine (~60%) and desformyl-methionine (~40%) forms of the protein are present in the sample (*41*). In this work, no distinction was made between the exchange rates for the formyl-methionine and desformyl-methionine proteins since analyses of resonances for S1, K5, and F43 for both forms yielded very similar rates.

A series of $^{1}H-^{15}N$ HSQC spectra for human apo-S100B were used to determine the individual amide exchange rates for the protein at pH 6.96 and 35 °C. Figure 2A shows the $^{1}H-^{15}N$ HSQC spectrum of the protein at pH 6.96 prior to exchange with D_2O. Upon lyophilization and rehydration with D_2O, there is little observable change in resonance positions. Figure 2B shows the spectrum of apo-S100B after a 10 h exchange period with D_2O. The 35 remaining resonances have slowed exchange rates and are all located in helices I (E4−H15 and Y17), II (L32−L40), and IV (F73−A83) and the linker (L44 and E45) of apo-S100B. No resonances from amides in helix III (Q50−D61) or in calcium-binding loop I (G19−E32) or II (D61−E72) are observed at the contour level shown (<1% original peak intensity). These observations show that in apo-S100B there is a clear distinction in the amide exchange rates between residues in helices I, II, and IV compared to residues in helix III and the calcium-binding loops.

A distinction in the amide exchange rates between residues in helices I, II, and IV compared to helix III is also found for Ca-S100B (Figure 3). For instance, after exchange with D_2O, resonances from helices I (E4−M7, L10, V13, F14, Q16, and Y17), II (L32−E39), and IV (F73, M74, and F76−M79) are still observable after 2 h. One predominant feature of the Ca-S100B exchange rates is that several residues from helices I (A9 and I11) and IV (A75, V80, and A83) exchange more quickly in this conformation than in the apo conformation. Also, only one residue (E58) is visible from helix III in Ca-S100B, despite the large rearrangement of this helix with respect to the remainder of the protein. Binding of calcium to S100B clearly alters some exchange rates in the calcium-binding sites as residues in calcium-binding sites I (S18, L27, and K28) and II (C68 and D69) are visible in Ca-S100B (Figure 3B) but are absent in the apo state (Figure 2B). Of these residues, L27, K28, C68, and D69 form a portion of the β-sheet between the two calcium-binding loops of the protein.

Amide Exchange Measurements. A series of rapidly conducted $^{1}H-^{15}N$ HSQC (*46*) experiments were used to follow amide exchange in human apo-S100B and Ca-S100B. For example, at pH 6.96, the dispersion of the $^{1}H-^{15}N$ correlations in apo-S100B, shown in Figure 2, allowed the amide exchange for 89 of 91 backbone resonances to be confidently followed for this protein using $^{1}H-^{15}N$ HSQC spectra measured as a function of time. Figure 4 shows several examples of amides in apo-S100B from different regions of the protein as having very distinct exchange properties. The best-fit curves shown are typical of all the data acquired for both apo- and Ca-S100B, yielding rate constants with a relative error of less than 5%. In apo-S100B, Figure 4 shows that residues located in calcium-binding loops I (K29) and II (D69) have the fastest amide decay rates. Significantly slower exchange is exhibited by residues in helix I (Y17) and helix IV (A83). Though these residues are among the fastest exchanging amides in these helices, their rates of exchange are easily discriminated from those of residues in helix III (V53).

For both conformations of S100B, residues that exhibited rates of exchange that were too fast to measure by the D_2O exchange out method were measured at pH 7.2 using the CLEANEX-PM method involving magnetization transfer from H_2O to exchangeable protons in the protein. The rates of exchange measured by this method ranged between 0.2 and 15.7 s^{-1}, covering ranges similar to those found for human acidic fibroblast growth factor (0.5−23.8 s^{-1}) (*59*) and the P43M mutant of calbindin D_{9k} (0.1−90 s^{-1}) (*60*). A total of 21 $^{1}H-^{15}N$ resonance peaks in apo-S100B and 7 in Ca-S100B could be measured in the CLEANEX-PM spectra even with low mixing times of 10 ms. In apo-S100B, most

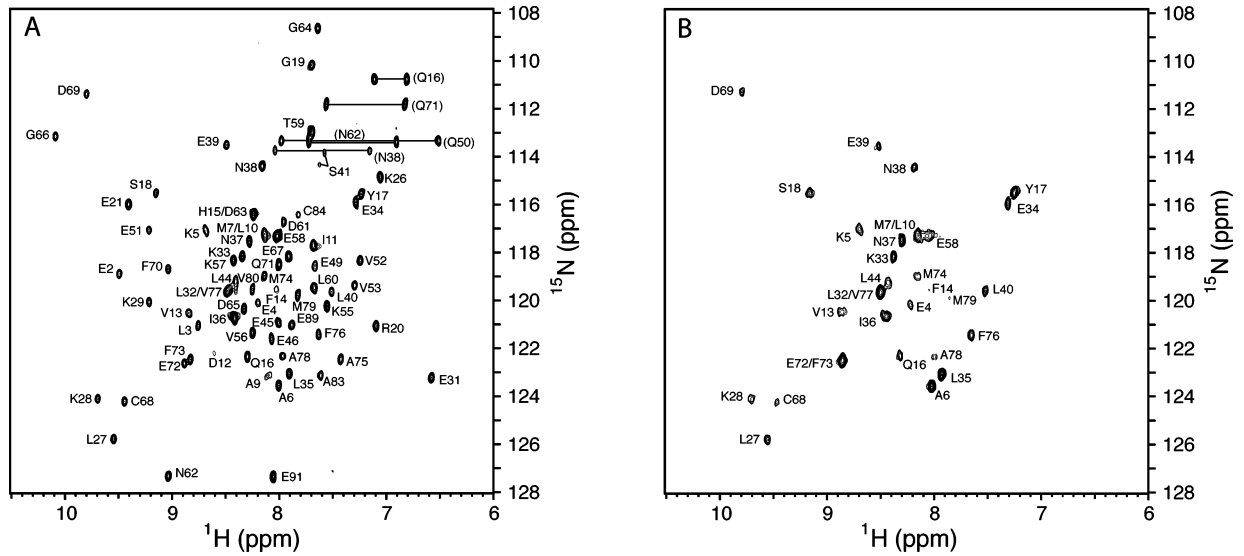

FIGURE 3: ^{1}H−^{15}N HSQC spectra of human Ca-S100B at pH 7.20 and 35 °C. Each spectrum is labeled with the amino acid number and letter code. Multiple forms (formyl-methionine and desformyl-methionine, described in the text) are present for K5. Spectrum A was acquired in a 90% H_2O/10% D_2O mixture immediately prior to deuterium exchange. Spectrum B was acquired after lyophilization of the sample in A and after the sample had been redissolved in D_2O and allowed to exchange for approximately 2 h at 35 °C. Spectrum B was plotted at 4 times the vertical scale of spectrum A.

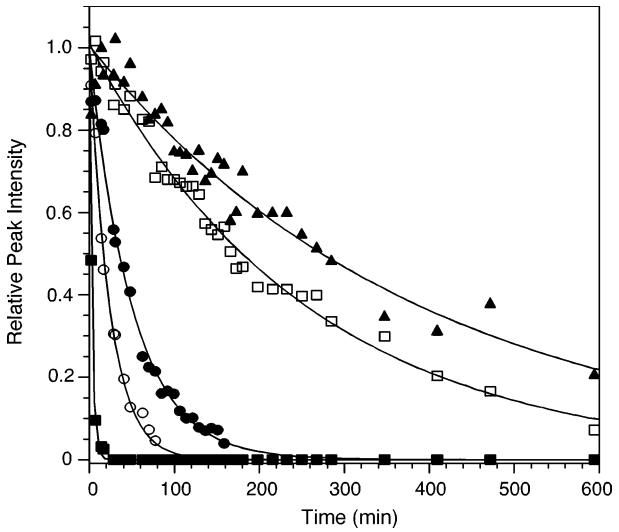

FIGURE 4: Analysis of amide exchange measurements. Peak intensities of selected amides from apo-S100B, plotted as a function of time, after addition of D_2O to the lyophilized protein. The plots show data for Y17 (▲) in helix I, K29 (■) in calcium-binding loop I, V53 (●) in helix III, D69 (○) in calcium-binding loop II, and A83 (□) in helix IV. In each case, the series of measured peak intensities were fit with a single-exponential decay curve as described in the text.

of the residues observed by CLEANEX-PM are found in helix III, the linker, and both calcium-binding loops. In contrast, there are no CLEANEX-PM resonances observed in the site II calcium-binding loop of Ca-S100B.

Helices I and IV Form a Dimeric Unfolding Unit in Apo-S100B. Protection factors (*61*) were used to express the measured exchange rates as this corrected for influences caused by the solvent (temperature, pH, and ionic strength) and the environment (sequence content) of the amide groups. Figure 5A shows the protection factors derived from measured exchange rates for apo-S100B at pH 6.96. In general, the log protection factors varied over a large range (from 0.37 to >7.0). The graph shows two prominent plateau regions are observed for helices I and IV in apo-S100B centered at L10/I11 in helix I and F76/V77 in helix IV. These are similar to the centers of these helices based on the three-dimensional structures of apo-S100B (*16*, *17*). These helices have an average log protection factor of ∼6.6. This corresponds to an unfolding free energy of ∼9.4 kcal/mol and agrees well with that obtained via chemical denaturation (8.7 ± 0.5 kcal/mol) based on effective monomer concentration (*62*, *63*). The unfolding free energy for apo-S100B is also similar to that obtained from amide exchange data for other well-behaved dimeric proteins such as Trp repressor (11.7 kcal/mol) (*64*) and the DNA-binding protein Sso10a (9.6 kcal/mol) (*65*), where the dimer interface is comprised mainly of α-helical interactions. Examination of apo-S100B structures determined from NMR studies (*16*, *17*) shows that residues within the plateau regions for helix I (A6, M7, L10, I11, V13, and F14) and helix IV (F73, M74, F76, V77, A78, V80, and T81) have more than 90% of their side chains protected from solvent (*19*, *62*). This trend of buried side chains is conserved within other S100 proteins such as apo-S100A11 (*55*) and the X-ray structures of apo-S100A3 (*28*) and apo-S100A6 (*22*). In addition, these structures have regular networks of well-defined hydrogen bonds characteristic of α-helices, including residues A6−G19 (helix I) and F73−T82 (helix IV) in apo-S100B (A8−G21 in both S100A3 and S100A6, Y75−H87 in S100A3, and Y73−L82 in S100A6). The leveling off of slow exchange rates near a helix center has been observed for several other proteins (*66*−*68*), including helices I and IV from apo-calbindin D_{9k} (shown in Figure 5B) (*39*), and is suggestive of a cooperative unfolding mechanism for the region composed of helices I and IV (I′ and IV′) in apo-S100B. This observation is consistent with the slowest exchanging amides in apo-S100B being a result of both well-defined hydrogen bonds and buried contact surfaces (*69*). These regions also have the highest degree of order in apo-S100B as indicated by ^{15}N relaxation studies (*34*).

Gradually decreasing protection factors for apo-S100B occur at the N- and C-termini of helices I (L3−K5 and Q16−

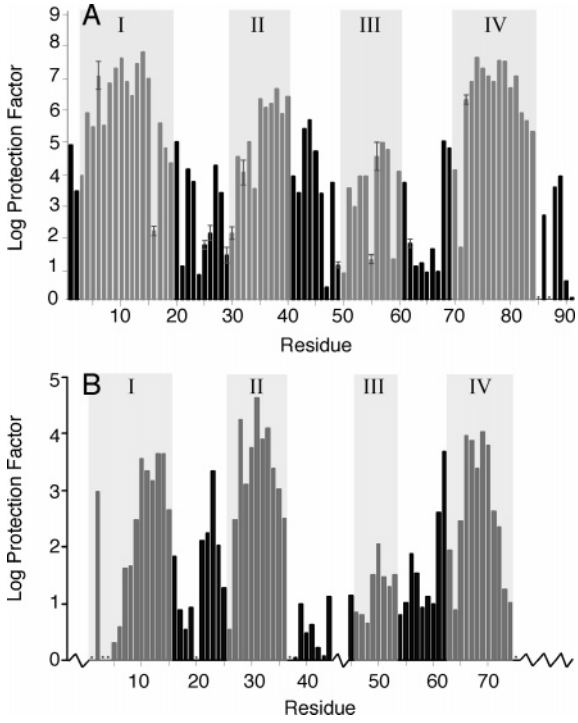

FIGURE 5: Comparison of apo-S100B and apo-calbindin D_{9k} amide protection factors. (A) Amide protection factors as a function of residue number for apo-S100B measured at 35 °C. (B) Apo-calbindin D_{9k} amide protection factors as determined by Skelton and co-workers (*39*). Both sets of protection factors were calculated using the measured rates and adjusted for the intrinsic rate as described by Bai et al. (*61*). Error bars are shown for protection factors of apo-S100B when measured exchange rates were associated with an error of >5%. The sequence of calbindin D_{9k} was aligned on the basis of the similarity of its sequence to that of S100B. Gaps within the sequence alignment of calbindin D_{9k} and S100B are shown with a crooked *x*-axis. Sequence alignments were completed with T-Coffee (*75*). Residues that could not be measured by amide exchange are represented with an asterisk above the unmeasured residue on each graph. Shaded areas on the two graphs represent the position of the helices within the corresponding protein.

G19), and IV (Q71, E72, and T82−C84). The apo-S100B structures (*16*, *17*) reveal residues at the N-termini of these two helices (E2 and L3, and F70 and Q71) are not hydrogen bonded. Similar trends of increased exchange rates toward the ends of helix I (K7, G8, A15, and K16) and helix IV (E65, K71, and K72) have been noted for apo-calbindin D_{9k} (*39*). In general, this behavior is consistent with a fraying of these helices toward their ends (*66*). The similarity of the exchange rates within each of the plateau regions, and the increased exchange rates near the ends of these helices, indicate that fraying of the helices does not proceed to the helix center.

Further comparison of apo-S100B and apo-calbindin D_{9k} (Figure 5) reveals the protection factors in helices I and IV in apo-S100B are nearly 3 orders of magnitude greater than those observed for the corresponding helices in apo-calbindin D_{9k} (*39*), the closest monomeric EF-hand relative to S100B. The higher protection factors found for helices I and IV in S100B most likely result from interactions at the dimer interface among helices I, I′, IV, and IV′, which are absent in monomeric calbindin D_{9k}.

Mobility of Helices II and III in Apo-S100B. The protection factors (*61*) for helices II and III are 1 and 3 orders of magnitude lower than those for helices I and IV in apo-S100B. Helix II shows a region of slow exchanging amides that includes L35−L40. On the basis of the structures of apo-S100B (*16*, *17*) and analogous X-ray structures for apo-S100A3 (*28*) and apo-S100A6 (*22*), these proteins have side chains that are >90% buried in helix II, including residues L35, I36, and L40 in S100B. The N-terminus of this helix (K29−E34) has much lower protection factors than the C-terminus, although a network of hydrogen bonds extends between L32 and L40 in apo-S100B ending abruptly at both N- and C-termini of this helix. This network of hydrogen bonds is also observed in apo-S100A3 and apo-S100A6. Also, on the basis of S100B structural data, the plateau center of helix II (N37/N38) is shifted by two to three residues from the helix center (E34/L35). In apo-S100B, the lower protection factor of K29−E34 likely results from more facile access to water based on the increased solvent accessibility (>50%) of residues K29, S30, K33, and E34. A comparison of the stabilities of helix II for calbindin D_{9k} and S100B is shown in Figure 5. In apo-calbindin D_{9k}, helix II has the highest protection factors, indicating it is the most stable region of the protein, compared to apo-S100B where helix II has protection factors at least 1 order of magnitude lower than those of helices I and IV. This subtle difference in amide exchange rates may be indicative of differing roles for helix II in apo-S100B (and other S100 proteins) and calbindin D_{9k} toward calcium binding.

In apo-S100B, helix III (Q50−D61) has the lowest protection factors of the four helices. A closer look at the protection factors in helix III shows that they take on a pyramidal shape, although residues K55 and T59 are anomalously low. These two residues have high surface accessibility, and the hydrogen bonds involving these two residues are longer than the optimal length, possibly resulting in the highest exchange rates within the helix. The pyramid-shaped trend of protection factors having a maximum at M57 is indicative of an unstable helix with fraying at both its N- and C-termini. This analysis is supported by the poor helical properties of helix III, which has fewer hydrogen bonds and is shorter (13 ± 1 residues) than helices I and IV. Helix III also has the smallest buried surface area of the four helices possessing only two residues, V56 and L60, that are buried to anchor this helix.

Overall Effects of Calcium Binding on Amide Exchange Rates. Protection factors were also used to express amide exchange rates in Ca-S100B (Figure 6A). A large range of protection factors was measured (from 0.21 to 7.21). In Ca-S100B, average log protection factors for helices I and IV found at the dimer interface were 5.2 and 4.6, respectively, ~2 orders of magnitude lower than that observed for apo-S100B. The decreased protection factors for helices I and IV are accompanied by a small increase in the protection factors for helix II in S100B, resulting in a similar protection factor average for helices I, II, and IV in Ca-S100B. The trend for protection factors for helices I, II, and IV for S100B is in contrast to that for Ca-calbindin D_{9k}, where helix II is the most stable helix in the apo (Figure 5B) and calcium-bound states (Figure 6B). As with apo-S100B, helix III remained the least protected of the helices in Ca-S100B, having protection values approximately 2.5 orders of magnitude lower than those of helices I, II, and IV.

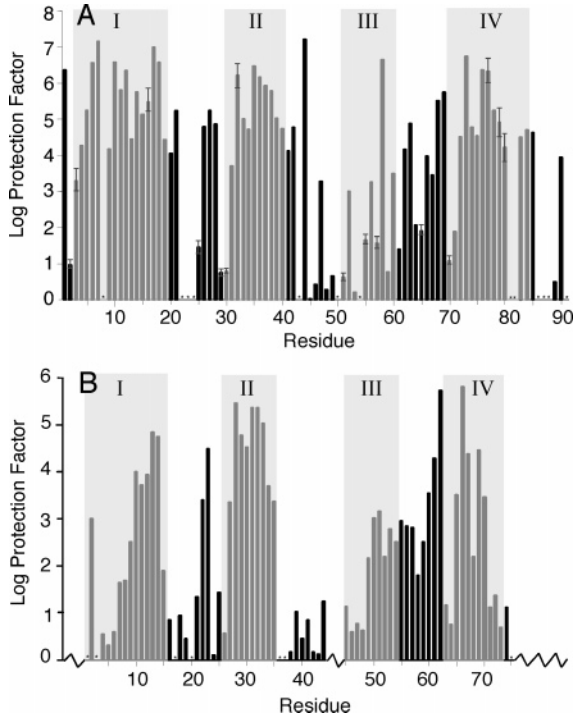

FIGURE 6: Comparison of Ca-S100B and Ca-calbindin D_{9k} amide protection factors. (A) Amide protection factors as a function of residue number for Ca-S100B measured at 35 °C. Error bars are included with the protection factors of Ca-S100B when measured exchange rates were associated with an error of >5%. (B) Ca-calbindin D_{9k} amide protection factors determined by Skelton and co-workers (*39*). The sequence alignment was completed and represented as in Figure 5. Residues that could not be measured are represented with an asterisk above the unmeasured residue on each graph. Shaded areas on the two graphs represent the position of the helices within the corresponding protein under these conditions.

Calcium Binding Leads to Lower Protection Factors in Helices II and III. To clearly define the impact of calcium binding and the conformational change involving helix III for S100B, the differences in protection factors between apo-S100B and Ca-S100B were plotted (Figure 7A). These were compared to changes observed for calbindin D_{9k} (Figure 7B), where repacking of helices III and IV is observed upon calcium binding. Despite significant differences in the structural response to calcium, and the absolute protection factors between these two proteins, the change in protection factors upon calcium binding reveals some striking similarities. For example, both proteins exhibit increased protection factors (1−2 orders of magnitude) throughout calcium-binding site II (S100B, N62−D69). This results from an ordering of this site that brings the side chains of D61, D63, and D65 into position to coordinate the calcium ion. As a result, the amide protons for residues in site II of Ca-S100B are directed toward the interior of the calcium-binding loop away from the surface of the protein. In addition, S100B and calbindin D_{9k} become more protected in the β-sheet portions of both sites I (S100B, K26−K28) and II (S100B, E67−D69). This is likely a result of the shortening and increased planarity of a pair of hydrogen bonds between L27 and C68 at the center of the β-sheet. The only other residue in site I having a significantly increased protection factor is E21, which experiences an ∼30% decreased accessible surface area upon calcium binding. These trends in protection factor differences between apo- and Ca-S100B are illustrated on the structure of Ca-S100B in Figure 7C.

The centers of helix II in Ca-S100B and helix II in Ca-calbindin D_{9k} undergo an increase in stability upon calcium binding. This effect appears to involve the entire helix II in calbindin D_{9k}, while in S100B, it is restricted to the five central residues (K33−N37). Interestingly, the C-terminus of helix II in S100B shows a decrease in protection factors in the calcium-bound state. This is coincident with a small increase in the accessible surface area in this region and the adjacent linker region that is important for interaction with biological targets in S100B, but not in calbindin D_{9k}.

The most obvious difference between protection factors for the apo and calcium-bound conformations is found in helix III. Binding of calcium to S100B leads to slower amide exchange for only one residue (E58) and more rapid exchange for others, whereas in calbindin D_{9k}, the six C-terminal residues (D54−G59) of helix III experience an increase in their protection factor. In S100B, this is accompanied by an increased level of exposure of many residues in helix III (Q50, E51, V56, and T59). This section of helix III has been shown to be critical for binding of target proteins such as TRTK-12 (*25*) and Ndr kinase (*26*). In calbindin D_{9k}, a nearly opposite affect is noted. Most of helix III (L46−D54) undergoes a decrease in its level of exposure, while only two residues at the center of helix II become less exposed. This is a result of repacking of helix III with helix IV in calbindin D_{9k} with little change in accessible surface area. This balance of protection factors between helices II and III may provide a key difference between S100B and calbindin D_{9k} with respect to the manner in which each responds to calcium. In S100B, the decreased protection factors of several helix III residues in combination with increased protection factors for a portion of helix II, upon calcium binding, result in differences between these helices of more than 4 orders of magnitude in response to calcium [the difference between positive bars in helix II and negative bars in helix III (Figure 7A)]. In contrast, binding of calcium to calbindin D_{9k} results in similar increases in protection factors for both helices II and III (Figure 7B) so that no net difference between these two helices is observed.

The protection factors noted for S100B in helix III, upon calcium binding, are consistent with observations in other proteins where a conformational change is required. For example, leghemoglobin (*70*) and T4 lysozyme (*71*) each have a helix (F-helix) that also undergoes a conformational change upon ligand binding. In leghemoglobin, the F-helix displays more rapid amide exchange in the apo form (*70*). Likewise, the L99A mutant of T4 lysozyme has faster amide exchange (*72*) and mobility on the microsecond to picosecond time scale (*71*) in its F-helix. In the S100 proteins, it is clear that helix III undergoes the largest conformational change (relative to the other helices) upon calcium binding. However, this structural change requires a significant repacking to take place with helix II. Thus, the protection factors of both helices II and III are affected by calcium binding in opposing manners (Figure 7C). In support of this idea, Maler and co-workers have noted that 69 contacts are modified between these helices (>3 Å) using distance difference matrices between apo- and Ca-S100B (*21*).

Calcium-Induced Conformational Changes Extend to the Dimer Interface. Four helices [I, I′, IV, and IV′ (Figure 1)]

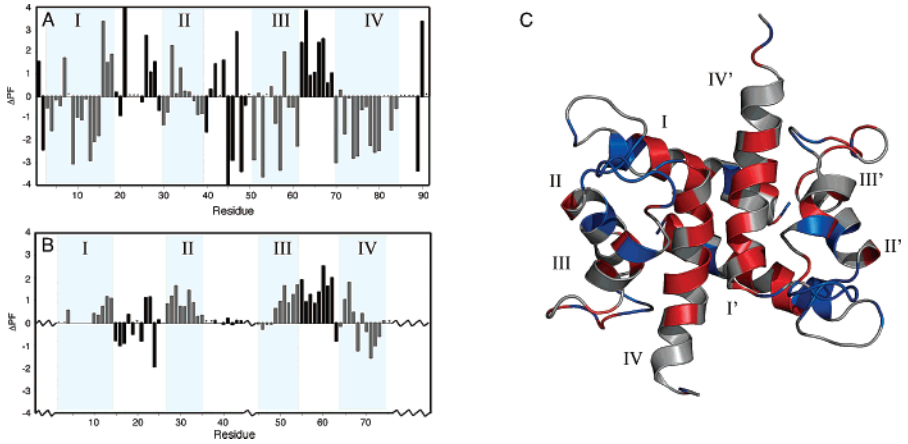

FIGURE 7: Difference in protection factors (ΔPF) for apo and calcium conformations of S100B and calbindin D_{9k}. (A) Bar graph showing the changes in log protection factor changes (ΔPF; see Experimental Procedures) for each residue upon binding of calcium to S100B. (B) Difference in protection factors for Ca- and apo-calbindin D_{9k}. In both panels A and B, positive bars denote increased protection from amide exchange for either Ca-S100B or Ca-calbindin D_{9k}. The sequence alignment is identical to that shown in Figures 5 and 6. Residues that could not be measured in either apo or calcium forms are represented with an asterisk above the unmeasured residue on each graph. Shaded areas on the two graphs represent the position of the helices within the corresponding protein. (C) Ribbon diagram of Ca-S100B (*13*) showing the differences in protection factors (ΔPF) for Ca- and apo-S100B. On the ribbon structure, a ΔPF of less than −1 (red) specifies the residue is more protected in the apo state. Also, a ΔPF of >1 (blue) is used to show the calcium state is more protected. Other residues that had smaller ΔPF values ($-1 < \Delta PF < 1$) are colored gray.

comprise the dimer interface of S100B. Binding of calcium to this protein results in protection factors decreased by 2−4 orders of magnitude (shown as negative bars in Figure 7A) in most of helices I and IV. This includes several residues between A9−H15 (helix I) and E72−C84 (helix IV) involved in the maintenance of the dimer interface. These observations are different from those for calbindin D_{9k}, where calcium binding either increases the protection factor by ∼1 order of magnitude (positive bars, Figure 7B) or has little effect on helix I. In helix IV of Ca-calbindin D_{9k}, calcium binding increases the protection factor of the N-terminal residues by up to 2 orders of magnitude while the C-terminal residues are oppositely affected by calcium binding (negative bars, Figure 7B).

These observations indicate that binding of calcium to S100B transmits structural changes to residues at the dimer interface of S100B (Figure 7C). Examination of apo and calcium-bound S100 structures reveals that calcium binding results in a small opening conformation by 9−18° (*29*) of helices I and I′, while the helix IV−helix IV′ interaction is modified by ∼6°. These smaller changes in orientation are largely overshadowed by the ∼40° change in helix III with respect to helices II and IV. In addition, binding of calcium to S100B exposes a large region toward the N-terminus of helix I (and I′) as a result of the reorientation of helix III (and III′) (*13*, *62*). In S100A11 and S100A10, this portion of the protein is important for interaction with target proteins such as annexins A1 and A2 (*23*, *27*, *55*).

In helix IV of S100B, the decreased protection factors between residues E72 and C84 involve residues at the dimer interface and those that are exposed for calcium-sensitive target protein interaction (Figure 7C). For example, residues A75 and V77−T82 at the dimer interface undergo an increase in their level of surface exposure upon calcium binding. Further, residues T82, A83, and E86−F88 within the T81−F88 region have an up to 6-fold higher accessible surface area in Ca-S100B than in apo-S100B, which is necessary for binding biological targets such as TRTK-12 (*73*), p53 (*74*), and Ndr kinase (*26*).

ACKNOWLEDGMENT

We thank Joanne Puzio who carried out some of the preliminary amide exchange experiments, Lewis Kay (University of Toronto, Toronto, ON) for advice and providing all pulse sequences, and Brian Sykes and Robert Boyko (University of Alberta, Edmonton, AB) for providing Xcrvfit. We thank Frank Delaglio and Dan Garrett (National Institutes of Health, Bethesda, MD) for NMRPipe and Pipp, Bruce Johnson for NMRView, and Dr. W. Englander for Excel spreadsheets used in the calculation of protection factors.

REFERENCES

1. Heizmann, C. W., Fritz, G., and Schafer, B. W. (2002) S100 proteins: Structure, functions and pathology, *Front. Biosci. 7*, d1356−d1368.
2. Donato, R. (2001) S100: A multigenic family of calcium-modulated proteins of the EF-hand type with intracellular and extracellular functional roles, *Int. J. Biochem. Cell Biol. 33*, 637−668.
3. Donato, R. (1988) Calcium-independent, pH-regulated effects of S-100 proteins on assembly-disassembly of brain microtubule protein in vitro, *J. Biol. Chem. 263*, 106−110.
4. Sorci, G., Agneletti, A. L., Bianchi, R., and Donato, R. (1998) Association of S100B with intermediate filaments and microtubules in glial cells, *Biochim. Biophys. Acta 1448*, 277−289.
5. Sorci, G., Agneletti, A. L., and Donato, R. (2000) Effects of S100A1 and S100B on microtubule stability. An *in vitro* study using triton-cytoskeletons from astrocyte and myoblast cell lines, *Neuroscience 99*, 773−783.
6. Bianchi, R., Giambanco, I., and Donato, R. (1993) S-100 protein, but not calmodulin, binds to the glial fibrillary acidic protein and inhibits its polymerization in a Ca^{2+}-dependent manner, *J. Biol. Chem. 268*, 12669−12674.
7. Bianchi, R., Garbuglia, M., Verzini, M., Giambanco, I., Ivanenkov, V. V., Dimlich, R. V., Jamieson, G. A., and Donato, R. (1996) S-100 (α and β) binding peptide (TRTK-12) blocks S-100/GFAP interaction: Identification of a putative S-100 target epitope within the head domain of GFAP, *Biochim. Biophys. Acta 1313*, 258−267.
8. Marshak, D. R., Pesce, S. A., Stanley, L. C., and Griffin, W. S. T. (1991) Increased S100b neurotrophic activity in Alzheimer's disease temporal lobe, *Neurobiol. Aging 13*, 1−7.
9. Van Eldik, L. J., and Griffin, W. S. T. (1994) S100b expression in Alzheimer's disease: Relation to neuropathology in brain regions, *Biochim. Biophys. Acta 1223*, 398−403.

10. Odink, K., Cerletti, N., Bruggen, J., Clerc, R. G., Tarcsay, L., Zwadlo, G., Gerhards, G., Schlegel, R., and Sorg, C. (1987) Two calcium-binding proteins in infiltrate macrophages of rheumatoid arthritis, *Nature 330*, 80−82.
11. Gagne, S. M., Tsuda, S., Li, M. X., Smillie, L. B., and Sykes, B. D. (1995) Structures of the troponin C regulatory domains in the apo and calcium-saturated states, *Nat. Struct. Biol. 2*, 784−789.
12. Ikura, M., Clore, G. M., Gronenborn, A. M., Zhu, G., Klee, C. B., and Bax, A. (1992) Solution structure of a calmodulin-target peptide complex by multidimensional NMR, *Science 256*, 632−638.
13. Smith, S. P., and Shaw, G. S. (1998) A novel calcium-sensitive switch revealed by the structure of human S100B in the calcium-bound form, *Structure 6*, 211−222.
14. Matsumura, H., Shiba, T., Inoue, T., Harada, S., and Kai, Y. (1998) A novel mode of target recognition suggested by the 2.0 Å structure of holo S100B from bovine brain, *Structure 6*, 233−241.
15. Drohat, A. C., Baldisseri, D. M., Rustandi, R. R., and Weber, D. J. (1998) Solution structure of calcium-bound rat S100B($\beta\beta$) as determined by nuclear magnetic resonance spectroscopy, *Biochemistry 37*, 2729−2740.
16. Drohat, A. C., Tjandra, N., Baldisseri, D. M., and Weber, D. J. (1999) The use of dipolar couplings for determining the solution structure of rat apo-S100B($\beta\beta$), *Protein Sci. 8*, 800−809.
17. Kilby, P. M., Van Eldik, L. J., and Roberts, G. C. (1996) The solution structure of the bovine S100B protein dimer in the calcium-free state, *Structure 4*, 1041−1052.
18. Potts, B. C. M., Smith, J., Akke, M., Macke, T. J., Okazaki, K., Hidaka, H., Case, D. A., and Chazin, W. J. (1995) The structure of calcyclin reveals a novel homodimeric fold for S100 Ca^{2+}-binding proteins, *Nat. Struct. Biol. 2*, 790−796.
19. Maler, L., Potts, B. C., and Chazin, W. J. (1999) High resolution solution structure of apo calcyclin and structural variations in the S100 family of calcium-binding proteins, *J. Biomol. NMR 13*, 233−247.
20. Sastry, M., Ketchem, R. R., Crescenzi, O., Weber, C., Lubienski, M. J., Hidaka, H., and Chazin, W. J. (1998) The three-dimensional structure of Ca^{2+}-bound calcyclin: Implications for Ca^{2+}-signal transduction by S100 proteins, *Structure 6*, 223−231.
21. Maler, L., Sastry, M., and Chazin, W. J. (2002) A structural basis for S100 protein specificity derived from comparative analysis of apo and Ca^{2+}-calcyclin, *J. Mol. Biol. 317*, 279−290.
22. Otterbein, L. R., Kordowska, J., Witte-Hoffmann, C., Wang, C.-L., and Dominguez, R. (2002) Crystal structures of S100A6 in the Ca^{2+}-free and Ca^{2+}-bound states: The calcium sensor mechanism of S100 proteins revealed at atomic resolution, *Structure 10*, 557−567.
23. Rety, S., Osterloh, D., Arie, J.-P., Tabaries, S., Seeman, J., Russo-Marie, F., Gerke, V., and Lewit-Bentley, A. (2000) Structural basis of the Ca^{2+}-dependent association between S100C (S100A11) and its target, the N-terminal part of annexin I, *Structure 8*, 175−184.
24. Barber, K. R., McClintock, K. A., Jamieson, G. A., Jr., Dimlich, R. V., and Shaw, G. S. (1999) Specificity and Zn^{2+} enhancement of the S100B binding epitope TRTK-12, *J. Biol. Chem. 274*, 1502−1508.
25. McClintock, K. A., Van Eldik, L. J., and Shaw, G. S. (2002) The C-terminus and linker region of S100B exert dual control on protein-protein interactions with TRTK-12, *Biochemistry 41*, 5421−5428.
26. Bhattacharya, S., Large, E., Heizmann, C. W., Hemmings, B., and Chazin, W. J. (2003) Structure of the Ca^{2+}/S100B/NDR kinase peptide complex: Insights into S100 target specificity and activation of the kinase, *Biochemistry 42*, 14416−14426.
27. Rety, S., Sopkova, J., Renouard, M., Osterloh, D., Gerke, V., Tabaries, S., Russo-Marie, F., and Lewit-Bentley, A. (1999) The crystal structure of a complex of p11 with the annexin II N-terminal peptide, *Nat. Struct. Biol. 6*, 89−95.
28. Fritz, G., Mittl, P. R., Vasak, M., Grutter, M. G., and Heizmann, C. W. (2002) The crystal structure of metal-free human EF-hand protein S100A3 at 1.7-Å resolution, *J. Biol. Chem. 277*, 33092−33098.
29. Smith, S. P., and Shaw, G. S. (1998) A change-in-hand mechanism for S100 signalling, *Biochem. Cell Biol. 76*, 324−333.
30. Linse, S., Brodin, P., Drakenberg, T., Thulin, E., Sellers, P., Elmden, K., Grundstrom, T., and Forsén, S. (1987) Structure-function relationships in EF-hand Ca^{2+}-binding proteins. Protein engineering and biophysical studies of calbindin D_{9k}, *Biochemistry 26*, 6723−6735.
31. Akke, M., Skelton, N. J., Kordel, J., Palmer, A. G., and Chazin, W. J. (1993) Effects of ion binding on the backbone dynamics of calbindin D_{9k} determined by ^{15}N NMR relaxation, *Biochemistry 32*, 9832−9844.
32. Barbato, G., Ikura, M., Kay, L. E., Pastor, R. W., and Bax, A. (1992) Backbone dynamics of calmodulin studied by ^{15}N relaxation using inverse detected two-dimensional NMR spectroscopy: The central helix is flexible, *Biochemistry 31*, 5269−5278.
33. Gagne, S. M., Tsuda, S., Spyrocopoulos, L., Kay, L. E., and Sykes, B. D. (1998) Backbone and methyl dynamics of the regulatory domain of troponin C: Anisotropic rotational diffusion and contribution of conformational entropy to calcium affinity, *J. Mol. Biol. 278*, 667−686.
34. Inman, K. G., Baldisseri, D. M., Miller, K. E., and Weber, D. J. (2001) Backbone dynamics of the calcium-signaling protein apo-S100B as determined by ^{15}N NMR relaxation, *Biochemistry 40*, 3439−3448.
35. Kordel, J., Skelton, N. J., Akke, M., Palmer, A. G., and Chazin, W. J. (1992) Backbone dynamics of calcium-loaded calbindin D_{9k} studied by two-dimensional proton-detected ^{15}N NMR spectroscopy, *Biochemistry 31*, 4856−4866.
36. Malmendal, A., Carlstrom, G., Hambraeus, C., Drakenberg, T., Forsen, S., and Akke, M. (1998) Sequence and context dependence of EF-hand loop dynamics. An ^{15}N relaxation study of a calcium-binding site mutant of calbindin D_{9k}, *Biochemistry 37*, 2586−2595.
37. Spyracopoulos, L., Lavigne, P., Crump, M. P., Gagne, S. M., Kay, C. M., and Sykes, B. D. (2001) Temperature dependence of dynamics and thermodynamics of the regulatory domain of human cardiac troponin C, *Biochemistry 40*, 12541−12551.
38. Spera, S., Ikura, M., and Bax, A. (1991) Measurement of the exchange rates of rapidly exchanging amide protons: Application to the study of calmodulin and its complex with a myosin light chain kinase fragment, *J. Biomol. NMR 1*, 155−165.
39. Skelton, N. J., Kordel, J., Akke, M., and Chazin, W. J. (1992) Nuclear magnetic resonance studies of the internal dynamics in apo, $(Cd^{2+})_1$ and $(Ca^{2+})_2$ calbindin D_{9k}, *J. Mol. Biol. 227*, 1100−1117.
40. Smith, S. P., Barber, K. R., Dunn, S. D., and Shaw, G. S. (1996) Structural influence of cation binding to recombinant human brain S100b: Evidence for calcium-induced exposure of a hydrophobic surface, *Biochemistry 35*, 8805−8814.
41. Smith, S. P., Barber, K. R., and Shaw, G. S. (1997) Identification and structural influence of a differentially modified N-terminal methionine in human S100b, *Protein Sci. 6*, 1110−1113.
42. Grzesiek, S., and Bax, A. (1992) An efficient experiment for sequential backbone assignment of medium-sized isotopically enriched proteins, *J. Magn. Reson. 96*, 432−440.
43. Kay, L. E., Ikura, M., Tschudin, R., and Bax, A. (1990) Three-dimensional triple-resonance NMR spectroscopy of isotopically enriched proteins, *J. Magn. Reson. 89*, 496−514.
44. Wittekind, M., and Mueller, L. (1993) HNCACB, a high-sensitivity 3D NMR experiment to correlate amide-proton and nitrogen resonances with the α- and β-carbon resonances, *J. Magn. Reson., Ser. B 101*, 171−180.
45. Zhang, O., Kay, L. E., Olivier, J. P., and Foreman-Kay, J. D. (1994) Backbone ^{1}H and ^{15}N resonance assignments of the N-terminal SH3 domains of drk in folded and unfolded states using enhanced-sensitivity pulsed field gradient NMR techniques, *J. Biomol. NMR 4*, 845−858.
46. Kay, L. E., Keifer, P., and Saarinen, T. (1992) Pure absorption gradient enhanced heteronuclear single quantum correlation spectroscopy with improved sensitivity, *J. Am. Chem. Soc. 114*, 10663−10665.
47. Delaglio, F., Grzesiek, S., Vuister, G. W., Zhu, G., Pfeifer, J., and Bax, A. (1995) NMRPipe: A multidimensional spectral processing system based on UNIX pipes, *J. Biomol. NMR 6*, 277−293.
48. Garrett, D. S., Powers, R., Gronenborn, A. M., and Clore, G. M. (1991) A common sense approach to peak picking in two-, three-, and four-dimensional spectra using automatic computer analysis of contour diagrams, *J. Magn. Reson. 95*, 214−220.
49. Johnson, B. A., and Belvins, R. A. (1994) NMRView: A computer program for the visualization and analysis of NMR data, *J. Biomol. NMR 4*, 603−614.

50. Smith, S. P., and Shaw, G. S. (1997) Assignment and secondary structure of calcium-bound human S100B, *J. Biomol. NMR 10*, 77−88.
51. Hwang, T. L., van Zijl, P. C., and Mori, S. (1998) Accurate quantitation of water-amide proton exchange rates using the phase-modulated CLEAN chemical EXchange (CLEANEX-PM) approach with a Fast-HSQC (FHSQC) detection scheme, *J. Biomol. NMR 11*, 221−226.
52. Hwang, T. L., Mori, S., Shaka, A. J., and van Zijl, P. C. M. (1997) Applications of phase-modulated CLEAN chemical EXchange spectroscopy (CLEANEX-PM) to detect water-protein proton exchange and intermolecular NOEs, *J. Am. Chem. Soc. 119*, 6203−6204.
53. Bai, Y., Milne, J. S., Mayne, L., and Englander, S. W. (1993) Primary structure effects on peptide group hydrogen exchange, *Proteins: Struct., Funct., Genet. 17*, 75−86.
54. Rustandi, R. R., Baldisseri, D. M., Inman, K. G., Nizner, P., Hamilton, S. M., Landar, A., Landar, A., Zimmer, D. B., and Weber, D. J. (2002) Three-dimensional solution structure of the calcium-signaling protein apo S100A1 as determined by NMR, *Biochemistry 41*, 788−796.
55. Dempsey, A. C., Walsh, M. P., and Shaw, G. S. (2003) Unmasking the annexin I interaction from the structure of Apo-S100A11, *Structure 11*, 887−897.
56. Vallely, K. M., Rustandi, R. R., Ellis, K. C., Varlamova, O., Bresnick, A. R., and Weber, D. J. (2002) Solution structure of human Mts 1 (S100A4) as determined by NMR spectroscopy, *Biochemistry 41*, 12670−12680.
57. Lee, Y. C., Volk, D. E., Thiviyanathan, V., Kleerekoper, Q., Gribenko, A. V., Zhang, S., Gorenstein, D. G., Makhatadze, G. I., and Luxon, B. A. (2004) NMR structure of the Apo-S100P protein, *J. Biomol. NMR 29*, 399−402.
58. Santamaria-Kisiel, L., Rintala-Dempsey, A. C., and Shaw, G. S. (2006) Calcium-dependent and -independent interactions of the S100 protein family, *Biochem. J. 396*, 201−214.
59. Chi, Y. H., Kumar, T. K., Kathir, K. M., Lin, D. H., Zhu, G., Chiu, I. M., and Yu, C. (2002) Investigation of the structural stability of the human acidic fibroblast growth factor by hydrogen-deuterium exchange, *Biochemistry 41*, 15350−15359.
60. Bertini, I., Carrano, C. J., Luchinat, C., Piccioli, M., and Poggi, L. (2002) A ^{15}N NMR mobility study on the dicalcium P43M calbindinD_{9k} and its mono-La^{3+}-substituted form, *Biochemistry 41*, 5104−5111.
61. Bai, Y., Milne, J. S., Mayne, L., and Englander, S. W. (1993) Primary structure effects on peptide group hydrogen exchange, *Proteins 17*, 75−86.
62. Ferguson, P. L., and Shaw, G. S. (2002) Role of the N-terminal helix I for dimerization and stability of the calcium-binding protein S100B, *Biochemistry 41*, 3637−3646.
63. Park, C., and Marqusee, S. (2004) Analysis of the stability of multimeric proteins by effective DeltaG and effective m-values, *Protein Sci. 13*, 2553−2558.
64. Finucane, M. D., and Jardetzky, O. (1996) The pH dependence of hydrogen-deuterium exchange in trp repressor: The exchange rate of amide protons in proteins reflects tertiary interactions, not only secondary structure, *Protein Sci. 5*, 653−662.
65. Kahsai, M. A., Vogler, B., Clark, A. T., Edmondson, S. P., and Shriver, J. W. (2005) Solution structure, stability, and flexibility of Sso10a: A hyperthermophile coiled-coil DNA-binding protein, *Biochemistry 44*, 2822−2832.
66. Wand, A. J., Roder, H., and Englander, S. W. (1986) Two-dimensional ^{1}H NMR studies of cytochrome c: Hydrogen exchange in the N-terminal helix, *Biochemistry 25*, 1107−1114.
67. Wagner, G. (1983) Characterization of the distribution of internal motions in the basic pancreatic trypsin inhibitor using a large number of internal NMR probes, *Q. Rev. Biophys. 16*, 1−57.
68. Yao, S., Smith, D. K., Hinds, M. G., Zhang, J. G., Nicola, N. A., and Norton, R. S. (2000) Backbone dynamics measurements on leukemia inhibitory factor, a rigid four-helical bundle cytokine, *Protein Sci. 9*, 671−682.
69. Vendruscolo, M., Paci, E., Dobson, C. M., and Karplus, M. (2003) Rare fluctuations of native proteins sampled by equilibrium hydrogen exchange, *J. Am. Chem. Soc. 125*, 15686−15697.
70. Morikis, D., and Wright, P. E. (1996) Hydrogen exchange in the carbon monoxide complex of soybean leghemoglobin, *Eur. J. Biochem. 237*, 212−220.
71. Mulder, F. A., Hon, B., Muhandiram, D. R., Dahlquist, F. W., and Kay, L. E. (2000) Flexibility and ligand exchange in a buried cavity mutant of T4 lysozyme studied by multinuclear NMR, *Biochemistry 39*, 12614−12622.
72. Llinas, M., Gillespie, B., Dahlquist, F. W., and Marqusee, S. (1999) The energetics of T4 lysozyme reveal a hierarchy of conformations, *Nat. Struct. Biol. 6*, 1072−1078.
73. McClintock, K. A., and Shaw, G. S. (2003) A novel S100 target conformation is revealed by the solution structure of the Ca^{2+}-S100B-TRTK-12 complex, *J. Biol. Chem. 278*, 6251−6257.
74. Rustandi, R. R., Drohat, A. C., Baldisseri, D. M., Wilder, P. T., and Weber, D. J. (1998) The Ca^{2+}-dependent interaction of S100B-($\beta\beta$) with a peptide derived from p53, *Biochemistry 37*, 1951−1960.
75. Notredame, C., Higgins, D. G., and Heringa, J. (2000) T-Coffee: A novel method for fast and accurate multiple sequence alignment, *J. Mol. Biol. 302*, 205−217.

BI6026242